ISIJ International, Vol. 52 (2012), No. 7, pp. 1225–1232

Modeling and Validation of the Radiative Heat Transfer in an Electric Arc Furnace

Vito LOGAR and Igor ŠKRJANC

Laboratory of Modeling, Simulation and Control, Faculty of Electrical Engineering, University of Ljubljana, Tržaška 25, Ljubljana, SI-1000 Slovenia. E-mail: vito.logar@fe.uni-lj.si, igor.skrjanc@fe.uni-lj.si

(*Received on January 23, 2012; accepted on February 22, 2012*)

This paper presents an approach to the mathematical modeling and validation of the radiative heat-transfer processes in an electric arc furnace (EAF). This radiative heat transfer represents an important part of the complete EAF model, which is further composed of electrical, hydraulic, thermal, chemical and mass-transfer sub-models. These have already been addressed in our previous publications. It is well known that during the operation of an EAF all three types of heat transfer (conductive, convective and radiative) are present; however, a great portion of the heat is transferred between the surfaces by means of radiation. The model presented in this work uses a simplified internal geometry of the EAF to represent the relations between the defined EAF zones and is developed in accordance with fundamental thermodynamic laws. The parameters of the model were fitted using the geometrical relations in the EAF; theoretically, using the conclusions from different studies involved in EAF modeling; and experimentally, using the measured temperatures on the furnace roof and the water-cooled panels. Since the radiative heat mostly represents a negative impact on the furnace roof, walls and linings, the obtained model represents an important part of the complete EAF. The presented results show satisfactory levels of similarity between the measured and simulated temperatures of the roof and water-cooled panels, which suggest that the presented model is relatively accurate and follows the fundamental laws of thermodynamics. Possessing such a model is of special importance when enhancing the EAF process using different optimization techniques, since the radiative impacts on the furnace need to be taken into the account in order to maintain or reduce the wear on the furnace lining.

KEY WORDS: EAF; electric arc furnace; radiative heat transfer; radiation model; view factors.

1. Introduction

The paper proposes an approach to the mathematical modeling of the radiative heat-transfer processes in a 3–phase, AC, electric arc furnace (EAF) and represents a part of a complete EAF model, which comprises the electrical, hydraulic, thermal, chemical and mass-transfer sub-models published in our previous papers.[1–3] The focus of the presented modeling work is to develop and present a relatively accurate and reliable relations that describe the radiative heat transfers between different zones of the EAF, such as the solid and liquid steel zones, the arcs, the roof and the walls. Some of these relations were indicated in the above mentioned papers in a shortened form; however, this study addresses them in greater detail, which allows the reader to replicate the work presented and clearly shows the variations of each quantity related to radiation during EAF operation. The radiative processes considered in this paper therefore include the radiative heat transfer dissipated from the arcs, steel, roof and walls and the corresponding view factors (VFs) between them. The later represent the most important part of the proposed radiative model, since the radiative energy inflows and outflows from EAF surfaces are directly dependent on the corresponding VFs between them. The obtained relations represent a significant part of the EAF thermal model, since up to 45% of the total input energy is transferred by means of radiation. Furthermore, the model's importance is extended due to the radiative wear of the furnace lining, which needs to be taken into account when operating or enhancing the EAF processes.

Modeling of the radiative processes in an EAF is seldom reported. Some limited information can be obtained from the paper of MacRosty and Swartz,[4] who proposed a model that considers the radiative heat exchange between the EAF surfaces -arcs, steel, roof and walls- where the model is founded on the simple internal geometry of the EAF. The presented idea of the furnace's division into zones is similar to MacRosty; however, there are some significant differences between the models, especially regarding the computation of the arcs' view factors, which determine the amount of radiation transferred from the arcs to the other surfaces. The distribution of the arcs' energy is important, since 70–80% of the electrical energy is transferred from the arcs in a radiative form.[5]

The developed model, presented in this paper, is based on an 80 MVA, AC furnace and is obtained in accordance with fundamental thermodynamic laws, with the parameters fitted using the geometrical relations in the EAF; theoretically,

using the conclusions from different studies involved in EAF modeling; and experimentally, using the online measured temperatures of the furnace roof and the water-cooled panels.

2. Modeling

To develop the radiative heat-transfer model the EAF layout was divided into several zones, where assumptions were made for all the zones to simplify the modeling of the processes. The assumptions that concern the proposed model are:

- The furnace layout is divided into 5 zones: 1 - roof, 2 - upper walls (water-cooled panels), 3 - solid steel, 4 - liquid steel and 5 - arcs.
- Each of the zones possesses similar characteristics regarding the physical properties, such as: emissivity, heat capacity, temperature, density, *etc*.
- All the surfaces/zones in the furnace are considered as simple geometric shapes, such as disks, rings, cylinders, cone-frustums, spheres or different combinations of these, with different orientations and positions relative to each other.
- During the melting process the geometric ratios between the surfaces change as a consequence of scrap melting and new scrap charging.
- Conductive heat transfer between the steel, the roof and the wall areas is neglected, since they are not in a direct contact. There is a short period of time at the beginning of each charge where the amount of solid steel is large enough to shield/touch the wall area. The shielded area of the walls is greater at the initial charge due to more steel usually being loaded. However, since in real practice the temperature of the solid steel is not equal throughout the whole volume as assumed here and can be in the contact area with the walls assumed similar to that of the walls (small temperature differences), the heat represented by conduction is small enough so that it can be ignored without significant loss of accuracy. Due to lower bulk density of the liquid steel in comparison to the solid steel, the height of the liquid phase is always bellow the slagline, which represents the transitional area between the furnace hearth and the furnace walls; meaning that due to the lack of a direct contact between the liquid steel and the walls, conduction does not occur. Similarly, the roof and the steel zones are never in a direct contact; therefore, no heat conduction occurs between them.

The geometry of the considered EAF and the typical phases of the meltdown process are shown in **Fig. 1**.

As shown in Fig. 1 there are four main phases of the scrap-melting process (for each furnace charge, typically 2 or 3) relevant for determining the different surface areas and the VFs between them. After the initial charge of the furnace, the electrodes bore themselves into the scrap, creating a cone-frustum-shaped void. As the melting progresses, the radius of the frustum increases and eventually reaches the edge of the furnace (phase 1). Afterwards, the frustum-shaped void starts to move downwards, exposing more and more of the wall's surface (phase 2). When a sufficient amount of scrap melts, the level of the liquid metal is reached by the arcs (phase 3). From this point on, the energy flow into the liquid metal increases, while the flow into the solid scrap decreases rapidly. When the melting process approaches an end, all of the scrap is molten and the slag starts to foam (phase 4). Variable dimensions of the zones are obtained from the mass-transfer model,[2] where the change of the mass is recalculated to the change of the volume and consequently to the change of radius, width and height of the specific zone. The computational methods presented in this paper ensure the continuous dynamics of the physical quantities when passing from one zone to another. The non-variable dimensions of the EAF are: $r_{eaf\ out}$ = 3.3 m, $r_{eaf\ in}$ = 2.45 m, r_{hole} = 1.7 m, $r_{electrode}$ = 0.3 m $h_{eaf\ up}$ = 2.9 m and $h_{eaf\ low}$ = 1.0 m. Nominal furnace steel capacity is 85.000 kg, with maximum capacity of 105.000 kg (including the additions).

All the needed parameters of the following model were addressed in Table 3 of our previous paper.[2]

2.1. Radiative Heat Transfer

It has already been mentioned that radiative heat transfer represents a significant amount of the total heat transferred in the EAF. As shown in Fig. 1, for the purpose of this study the furnace is considered as an enclosure with 5 surfaces (roof = ring, walls = cylinder, steel scrap = cone frustum

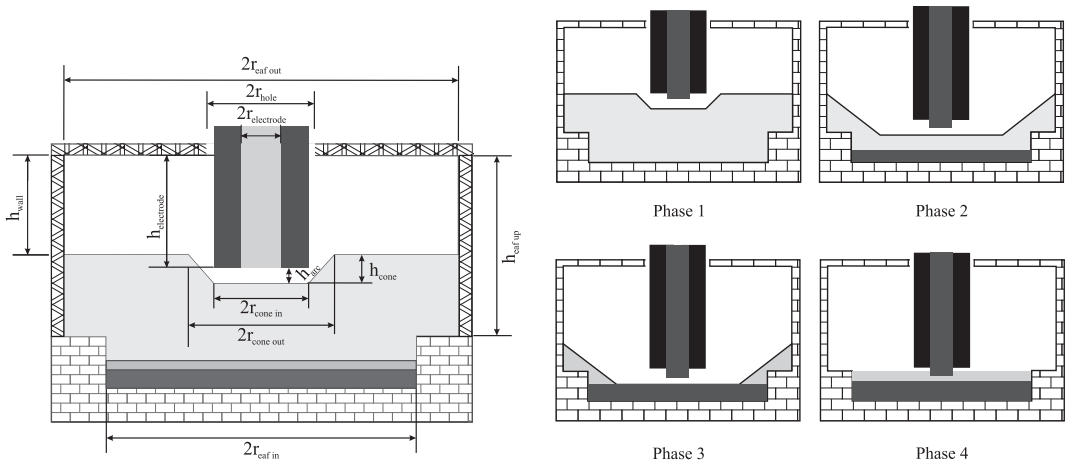

Fig. 1. Left panel: Geometry of the studied EAF with hatched areas denoting furnace roof, wall and hearth areas; Right panel: Four different phases of the scrap-melting process relevant for obtaining the surface areas and view factors.

attached to coaxial ring, liquid metal = disk, arcs = cylinders), treated as gray bodies. To determine the radiative energy input or output from a given surface gray-body the radiosity J_i needs to be determined with the Eq. (1):[6]

$$J_i = \varepsilon_i \sigma_{SB} T_i^4 + (1-\varepsilon_i)\sum_{j=1}^{N}(VF_{ij} \cdot J_j), \quad \text{..... (1)}$$

where ε_i represents the surface emissivity [0-1], σ_{SB} represents the Stefan-Boltzmann constant, T_i represents the body temperature, VF_{ij} represents the view-factor from surface i to surface j [0-1] and J_j represents the radiosity of the body j. The first part of Eq. (1) represents the gray-body radiation according to the Stefan-Boltzmann law, while the second part of the equation represents the incident radiation, which is the sum of the radiations from all the other surfaces per unit of surface area i. By obtaining the radiosity for all the bodies in the furnace, the radiative heat transfer Q_{i-RAD} for the surface i can be computed with Eq. (2):[6]

$$Q_{i-RAD} = A_i \sum_{j=1}^{N} VF_{ij}(J_i - J_j), \quad \text{..... (2)}$$

where A_i represents the surface i area, VF_{ij} represents the VF from surface i to surface j and J_i and J_j represent the radiosities of surfaces i and j, respectively. The radiative heat transfer can be positive or negative, where the former represents the loss of radiative energy, while the latter represents the reception of radiative energy.

The VFs that are needed in the radiative heat-transfer Eqs. (1) and (2) were obtained from different sources that have studied radiative heat transfer,[6–12] assuming that the inner zones of the EAF are simple geometrical shapes. The dimensions of all 5 zones tend to change during the melting process from either the initial non-zero value to the end zero, from the initial zero to the end non-zero or from the initial to the end non-zero values. Taking this into account and using the above equations the radiative heat transfer between all 5 EAF zones can be obtained. The arcs are considered as black bodies and transparent when receiving the radiative energy.

2.2. View Factors and Surface Areas

As Eqs. (1) and (2) suggest, the amount of radiative heat transfer between the surfaces is dependent on the surface emissivities, temperatures, surface areas and VFs from one surface to another. At this point the relations between the VFs, the surface areas and the geometry of the furnace and the steel are considered. Since the EAF is an enclosure with N surfaces the sum of all the VFs from one surface to the others is 1 and by definition a view-factor reciprocity rule applies between two surfaces, as given by Eq. (3):

$$\sum_{j=i}^{N} VF_{i-j} = 1$$
$$A_i \cdot VF_{i-j} = A_j \cdot VF_{j-i}, \quad \text{..... (3)}$$

meaning that a VF from surface i to j equals the VF from surface j to i multiplied by the ratio of the surface areas $\frac{A_j}{A_i}$. The definitions in Eq. (3) are useful when determining the VFs between complex surfaces (*i.e.*, arcs to steel), as they can be obtained from other VFs in an enclosure, which are easier to obtain. Further on, in some cases in sections 2.2.1 and 2.2.2, the main VF (VF_{i-j}) is, due to complex zone shapes or its composition of more than one shape, calculated using two related easily obtainable VFs ($VF_{i-j,x}$), where the suffix x denotes the number of the corresponding auxiliary VF, using the above reciprocity rule.

2.2.1. View Factors from Arcs

Since the energy dissipated from the electric arcs prevails in a radiative form, the VFs from the arcs to other surfaces in the furnace play a significant role. When considering the situation prior to the flat bath, *i.e.*, solid scrap is present, the VFs from the arc tend to change as the scrap melts and are harder to determine. It is generally known that the electrodes bore into the scrap at the beginning of each charge, meaning that the VF from the arc to the scrap increases in proportion to the electrode's progress into the scrap and then gradually decreases when the scrap surrounding the electrode melts.

The view factor VF_{5-1} can be obtained using the geometric relation between the outer surface of the cylinder (arc) to the axial annular ring (roof) at a certain distance from the cylinder using Eqs. (4), (5) and (6):[8,10,11]

$$VF_{5-1,1} = \frac{B_1}{8RH_1} + \frac{1}{2\pi}\left(a\cos\frac{A_1}{B_1} - \frac{1}{2H_1}\left(\sqrt{\frac{(A_1+2)^2}{R^2}-4}\right)\cdot a\cos\frac{A_1 R}{B_1} - \frac{A_1}{2RH_1}\cdot a\sin R\right)$$

$$R = r_{electrode} / r_{eaf\ out};\ H_1 = (h_{electrode} + h_{arc}) / r_{eaf\ out}$$

$$A_1 = H_1^2 + R^2 - 1;\ B_1 = H_1^2 - R^2 + 1, \quad \text{..... (4)}$$

where $r_{electrode}$ represents the electrode radius, $r_{eaf\ out}$ represents the radius of the furnace roof, h_{arc} represents the arc length and $h_{electrode}$ represents the variable length of the electrodes in the furnace. VF in Eq. (4) assumes the arcs are attached to the roof; however, since the arcs are not attached to the roof, the $VF_{5-1,1}$ has to be decreased by the VF represented by the electrodes' length using Eq. (5):

$$VF_{5-1,2} = \frac{B_2}{8RH_2} + \frac{1}{2\pi}\left(a\cos\frac{A_2}{B_2} - \frac{1}{2H_2}\left(\sqrt{\frac{(A_2+2)^2}{R^2}-4}\right)\cdot a\cos\frac{A_2 R}{B_2} - \frac{A_2}{2RH_2}\cdot a\sin R\right)$$

$$R = r_{electrode} / r_{eaf\ out};\ H_2 = (h_{electrode}) / r_{eaf\ out}$$

$$A_2 = H_1^2 + R^2 - 1;\ B_2 = H_1^2 - R^2 + 1, \quad \text{..... (5)}$$

where the appearing dimensions are presented in Fig. 1.

In this manner the main VF from the arcs to the roof can be obtained from Eq. (6):

$$VF_{5-1} = \frac{VF_{5-1,1} \cdot A_{5-1,1} - VF_{5-1,2} \cdot A_{5-1,2}}{A_{5-1,3}}, \quad \text{..... (6)}$$

where $A_{5-1,1}$ represents the surface area of the cylinder extending from the roof to the steel surface, $A_{5-1,2}$ represents the surface area of the electrodes and $A_{5-1,3}$ represents the surface area of the arc.

The view factor VF_{5-2} can be obtained using the geometric relation between the cylinder (arc) positioned on the same axis inside or stretching outside the bigger radial cylinder (walls). The position of the arcs in relation to the walls is dependent on the bore-down electrode depth in the steel, while the VF can be obtained with Eq. (7)[11,12] (arcs outside or partially submerged in the steel) or Eq. (10)[11] (arcs completely submerged in the steel):

$$VF_{5-2}=\frac{X}{L}F_X+\frac{L-X}{L}(1-F_{L-X})+\frac{Y+X-L}{L}F_{Y+X-L}-\frac{X+Y}{L}F_{X+Y}, \quad \text{..... (7)}$$

where the coefficients F_X, F_{L-X}, F_{Y+X-L} and F_{X+Y} can be obtained with Eq. (8):

$$F_\zeta=\frac{B_\zeta}{8R\zeta}+\frac{1}{2\pi}\left(a\cos\frac{A_\zeta}{B_\zeta}-\frac{1}{2\zeta}\left(\sqrt{\frac{(A_\zeta+2)^2}{R^2}-4}\right)\cdot a\cos\frac{A_\zeta R}{B_\zeta}-\frac{A_\zeta}{2R\zeta}\cdot a\sin R\right), \quad \text{..... (8)}$$

where ζ equals X, $L-X$, $Y+X-L$ or $X+Y$ obtainable with Eq. (9):

$$X=h_{cone}/r_{eaf\ out};\ Y=h_{wall}/r_{eaf\ out};\quad L=h_{arc}/r_{eaf\ out},\ R=r_{electrode}/r_{eaf\ out} \quad \text{..... (9)}$$
$$A_\zeta=\zeta^2+R^2-1,\ B_\zeta=\zeta^2-R^2+1$$

where the necessary dimensions are presented in Fig. 1.

When the arcs are completely submerged in the steel the VF can be obtained by Eq. (10):[11]

$$VF_{5-2}=\frac{L+D}{L}F_{L+D}+\frac{Y+D}{L}F_{Y+D}-\frac{D}{L}F_D-\frac{L+D+Y}{L}F_{L+D+Y}, \quad \text{..... (10)}$$

where the coefficients F_{L+D}, F_{Y+D}, FD and F_{L+D+Y} can be obtained with Eq. (8), where ζ equals $L+D$, $Y+D$, D or $L+D+Y$, obtainable with Eq. (11):

$$D=(h_{wall}+h_{cone}-h_{arc})/r_{eaf\ out};\ Y=h_{wall}/r_{eaf\ out};\quad L=h_{arc}/r_{eaf\ out},\ R=r_{electrode}/r_{eaf\ out} \quad \text{.... (11)}$$

where the dimensions are presented in Fig. 1.

With the VFs from the arcs to the roof (VF_{5-1}) and the walls (VF_{5-2}) defined, it is relatively simple to obtain the VF from the arcs to the solid (VF_{5-3}) or liquid steel (VF_{5-4}) using the reciprocity rule with Eq. (12):

$$VF_{5-3}=(1-VF_{5-1}-VF_{5-2})\cdot\left(1-K_{sSc-lSc}\left(1-\frac{m_{sSc}}{m_{charge}}\right)\right)$$
$$VF_{5-4}=(1-VF_{5-1}-VF_{5-2})\cdot\left(K_{sSc-lSc}\left(1-\frac{m_{sSc}}{m_{charge}}\right)\right), \quad \text{..... (12)}$$

where the product $K_{sSc-lSc}\left(1-\frac{m_{sSc}}{m_{charge}}\right)$ is the exposure coefficient [0-1], which determines the exposure of the solid (*sSc*) or liquid metal (*lSc*). $K_{sSc-lSc}$ is approximated as a tangenthyperbolic function from the amount of solid and liquid metal (height), and denotes when the arcs reach the liquid metal, while $\left(1-\frac{m_{sSc}}{m_{charge}}\right)$ approximates the exposure of the liquid surface in comparison to the solid steel, where m_{sSc} represents the solid steel mass and m_{charge} represents the total amount of steel charged at each basket. Exposure coefficient has also been addressed in our previous papers.[2,3] Since the assumption has been made that arcs do not receive radiative energy, the VFs from other surfaces to the arcs are not needed.

2.2.2. Other View Factors

To determine all the radiative heat impacts in the EAF, the VFs between other surfaces in the furnace are also important, since the temperatures of the steel reach up to 1 900 K. The VF between the solid steel and the roof (VF_{3-1}) and vice versa (VF_{1-3}) can be determined using two auxiliary VFs describing a ring attached to a cone-frustum (solid steel) opposed to the coaxial ring (roof) by Eqs. (13) (ring to ring) - $VF_{1-3,1}$ and (15) (cone-frustum to ring) - $VF_{1-3,2}$:[9]

$$VF_{1-3,1}=\frac{1}{2(R_2^2-1)}\left(\sqrt{(R_2^2+R_3^2+H^2)^2-(2R_3R_2)^2}-\sqrt{(R_2^2+R_4^2+H^2)^2-(2R_2R_4)^2}+\sqrt{(1+R_4^2+H^2)^2-(2R_4^2)^2}-\sqrt{(1+R_3^2+H^2)^2-(2R_3^2)^2}\right), \quad \text{... (13)}$$

where the coefficients R and H can be obtained with Eq. (14):

$$H=h_{wall}/r_{hole};\ R_2=r_{eaf\ out}/r_{hole};\quad R_3=r_{cone\ out}/r_{hole};\ R_4=r_{eaf\ out}/r_{hole}, \quad \text{..... (14)}$$

with the appearing dimensions presented in Fig. 1.

To obtain the VF from the cone-frustum to the ring, first the VF from cone-frustum to its base needs to be obtained with Eq. (15):

$$VF_{1-3,2}=\frac{2R^2-X+\sqrt{X^2-4R^2}}{2\sqrt{X-2R}(1+R)}, \quad \text{..... (15)}$$

where H, R and X can be obtained with Eq. (16):

$$H=h_{cone}/r_{cone\,in};\ R=r_{cone\,out}/r_{cone\,in};\ X=1+R^2+H^2, \quad \text{.... (16)}$$

with the appearing dimensions presented in Fig. 1. With the VF from the cone-frustum to its base obtained, the relation between the cone-frustum and the roof can be determined by multiplication of the $VF_{1-3,2}$ with the VF from the cone-frus-

tum base to the roof (disk to ring), which is calculated with Eq. (18) (with the appearing coefficients defined as $H = h_{wall} / r_{cone\ out}$; $R_2 = r_{hole} / r_{cone\ out}$; $R_3 = r_{eaf\ out} / r_{cone\ out}$). The view factors VF_{1-3} and VF_{3-1} are therefore determined with Eq. (17):

$$VF_{1-3} = VF_{1-3,1} + VF_{1-3,2} \cdot VF_{4-1}$$
$$VF_{3-1} = VF_{1-3} \frac{A_1}{A_3}, \quad \text{..... (17)}$$

where A_1 and A_3 are the surface areas of the roof and the solid steel, respectively.

The VFs from the liquid steel (disk) to the roof (ring), *i.e.*, VF_{4-1} and vice versa VF_{1-4}, can be obtained with Eq. (18):[7]

$$VF_{4-1} = \frac{1}{2}\left(R_3^2 - R_2^2 - \sqrt{(1+R_3^2+H^2)^2 - 4R_3^2} + \sqrt{(1+R_2^2+H^2)^2 - 4R_2^2}\right)$$
$$VF_{1-4} = VF_{4-1} \frac{A_4}{A_1}, \quad \text{.... (18)}$$

where A_1 and A_4 are the surface areas of the roof and the liquid steel, respectively, and the coefficients R and H can be obtained from Eq. (19):

$$H = h_{wall} / r_{eaf\ in};\ R_2 = r_{hole} / r_{eaf\ in};\ R_3 = \frac{r_{eaf\ out}}{r_{eaf\ in}}, \quad \text{... (19)}$$

with the appearing dimensions presented in Fig. 1.

The VF from the solid steel (ring attached to a cone-frustum) to the walls (cylinder) can also be described using two additional VFs. The first auxiliary VF, *i.e.*, $VF_{3-2,1}$ can be obtained using the already-described VF (cone-frustum to its base) in Eq. (15), multiplied by the VF from the disk to the outside cylinder, as shown in Eq. (20). In this manner, a frustum portion of the solid scrap to the walls is covered:

$$VF_{3-2,1} = VF_{1-3,2} \cdot \frac{1}{2}\left(1 - R^2 - H^2 + \sqrt{(1+R^2+H^2)^2 - 4R^2}\right), \quad \text{..... (20)}$$

where R and H can be obtained by Eq. (21):

$$R = r_{eaf\ out} / r_{cone\ out};\ H = h_{wall} / r_{cone\ out}, \quad \text{..... (21)}$$

with the appearing dimensions presented in Fig. 1.

The remaining part of the VF from the solid steel (ring) to the walls (cylinder), *i.e.*, $VF_{3-2,2}$ can be obtained with Eq. (22):

$$VF_{3-2,2} = \frac{1}{2}\left(1 + \frac{1}{R^2-1}\left[H\sqrt{4R^2+H^2} - \sqrt{(1+R^2+H^2)^2 - 4R^2}\right]\right), \quad \text{..... (22)}$$

where R and H are defined by Eq. (21) and the defined dimensions correspond to Fig. 1. The VFs from the solid steel to the walls VF_{3-2} and vice versa VF_{2-3} can thus be obtained with Eq. (23)

$$VF_{3-2} = VF_{3-2,1} + VF_{3-2,2}$$
$$VF_{2-3} = VF_{3-2} \frac{A_3}{A_2}, \quad \text{..... (23)}$$

where A_2 and A_3 are the surface areas of the walls and the solid steel, respectively.

The VFs from the liquid steel (disk) to the walls (cylinder) and vice versa, *i.e.*, VF_{4-2} and VF_{2-4}, can be obtained using Eq. (24):[9]

$$VF_{4-2} = \frac{1}{2}\left(1 - R^2 - H^2 + \sqrt{(1+R^2+H^2)^2 - 4R^2}\right)$$
$$VF_{2-4} = VF_{4-2} \frac{A_4}{A_2}, \quad \text{..... (24)}$$

where R and H are defined as Eq. (25):

$$R = r_{eaf\ out} / r_{eaf\ in};\ H = h_{wall} / r_{eaf\ in}, \quad \text{..... (25)}$$

with the appearing dimensions presented in Fig. 1.

The view factors VF_{5-1}, VF_{5-2}, VF_{1-4}, VF_{4-1}, VF_{2-4} and VF_{4-2} are (before calculating VFs VF_{5-3} and VF_{5-4}) multiplied by the coefficient $(1 - K_{slag})$ [0 – 1], which denotes a decrease in the VFs with the increasing height of the slag h_{slag} and can be obtained with Eq. (26):[3,13]

$$K_{slag} = 0.7\left(\frac{1}{2}\tanh(5h_{slag} - 1.25) + \frac{1}{2}\right)\left(\frac{1}{2}\tanh\left(3.2\left(1 - \frac{m_{sSc}}{m_{charge}}\right) - 1.29\right) + \frac{1}{2}\right), \quad \text{.... (26)}$$

where h_{slag} is the slag height, m_{sSc} is the current mass of solid steel and m_{charge} is the initial mass of the steel scrap loaded during each charge.

Since the impact from the furnace roof to the walls is small due to the low temperatures of the surfaces, the equations defining the view factors VF_{2-1} and VF_{1-2} are not included in this paper. Similarly, the VFs between the solid and liquid steels (VF_{4-3} and VF_{3-4}) are neglected as these zones are in direct contact, where conductive heat transfer prevails. Also, the VFs from one surface to itself are neglected, since the energy input and output to that surface is equal and does not affect the surface temperature.

With the VFs, surface areas and radiative heat transfers defined, the cooling-water temperatures of the roof (composed of alumina and steel) and walls (composed of steel) can be computed using Eqs. (39) and (40) of our previous study.[2]

3. Results and Discussion

The following section presents the relevant results obtained from the developed radiation model, which is a part of the complete EAF model that has already been addressed.[1–3] In this manner, the results relevant to the radiative heat transfer are shown, while other results are omitted and can be accessed in the previously mentioned publications. Similarly, the results shown are obtained using the same simulation and measurement timeline; however, only radiation is considered in the condition of Table 1[2] for this study. Meaning, that all other values (masses and temperatures) are exactly the same as in the before mentioned paper.

Figure 2 shows the VFs' dynamics during the melting period from the arcs to other surfaces in the EAF and the exposure coefficient $K_{sSc-lSc}\left(1 - \frac{m_{sSc}}{m_{charge}}\right)$, which influences

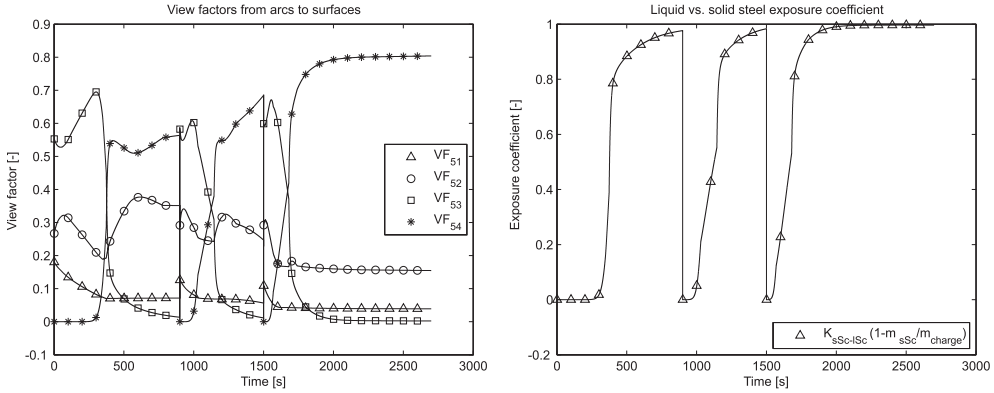

Fig. 2. Left panel: View factors from arcs to other surfaces in the EAF; Right panel: Exposure coefficient [0-1]; 0 - all radiative heat transferred to solid steel; 1 - all radiative heat transferred to liquid steel.

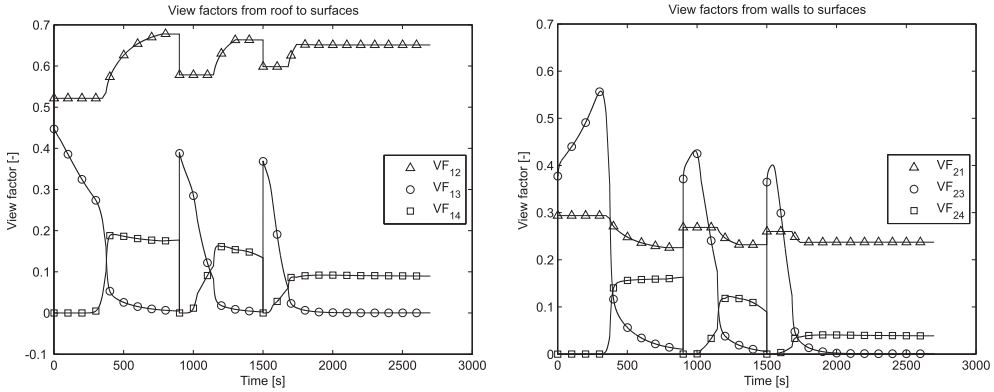

Fig. 3. Left panel: View factors from the roof to other surfaces in the EAF; Right panel: View factors from the walls to other surfaces in the EAF.

the distribution of the arcs' radiative heat to either solid or liquid zone described in Eq. (12).

As can be seen in Fig. 2, at time 0 s the VFs from the arcs to the roof ($VF_{5–1}$) and walls ($VF_{5–2}$) start to decrease, while the VF from the arcs to the solid steel ($VF_{5–3}$) starts to increase, which is a consequence of the electrode bore-down into the solid steel. As the electrode progresses into the scrap, the surrounding scrap is shielding the arcs, which results in a lower $VF_{5–1}$ and $VF_{5–2}$ and a higher $VF_{5–3}$. When sufficient amount of the steel melts the cone-frustum void becomes deep enough for the arcs to reach the liquid steel phase and to expose the liquid bath underneath (around 300 s, 1 200 s and 1 600 s), which increases the exposure coefficient and consequently the VF from the arcs to the liquid steel ($VF_{5–4}$). Simultaneously, the VF from the arcs to the solid steel ($VF_{5–3}$) starts to drop rapidly. Since the lower radius of the frustum is already large enough and a large amount of the solid steel is molten, exposure coefficient quickly reaches values around 0.8 and gradually raises to 1 when all the steel melts or is already submerged in the liquid bath. Similarly, as the solid steel is melting more wall area is exposed to the arcs' impact, which can be observed between times 300 s and 900 s and between times 1 200 s and 1 500 s. At times 900 s and 1 500 s a sharp increase in $VF_{5–3}$ and a sharp decrease in $VF_{5–4}$ are visible, which is a consequence of the new basket charge, meaning that the bath is again covered by the solid steel and the electrodes need to bore into the scrap to reach the liquid phase and expose the walls. From times 600 s to 900 s, 1 200 s to 1 500 s and from 1 600 s to 2 200 s a decrease in all the VFs except $VF_{5–4}$ is visible, which is a consequence of the slag-foaming process, described in Eq. (26). Foaming slag covers the arcs and decreases their radiative impact on the roof and walls, but diverts their energy to the steel instead. What is also observable from Fig. 2 is that the dynamics of the exposure coefficient directly influence the distribution of the arcs' view factors and consequently the radiative heat between the solid and the liquid steel zones.

Figure 3 represents the VFs from the roof and walls to other surfaces in the EAF, respectively.

As can be seen in Fig. 3 a sharp increase followed by a gradual decrease in VFs from the roof $VF_{1–3}$ and walls $VF_{2–3}$ to the solid steel appears during each furnace charge, which is a consequence of loading the solid steel followed by the bore-down of the electrodes. On the other hand, the VF from the roof to the walls $VF_{1–2}$ starts to increase after each charge, which is a consequence of the steel melting and more wall being exposed. The $VF_{2–1}$ decreases in proportion to the increase of $VF_{1–2}$, since the surface of the exposed walls is increasing. Also visible towards the end of the melting process are much lower values of $VF_{1–4}$ and $VF_{2–4}$, compared to the beginning, which is due to the foaming slag covering the liquid steel and limiting its radiative heat impact on the roof and the walls.

Figure 4 shows the VFs from the solid and liquid steels to the roof and walls of the EAF.

As seen in Fig. 4 during each furnace charge a sharp increase followed by a gradual decrease in $VF_{3–1}$ can be

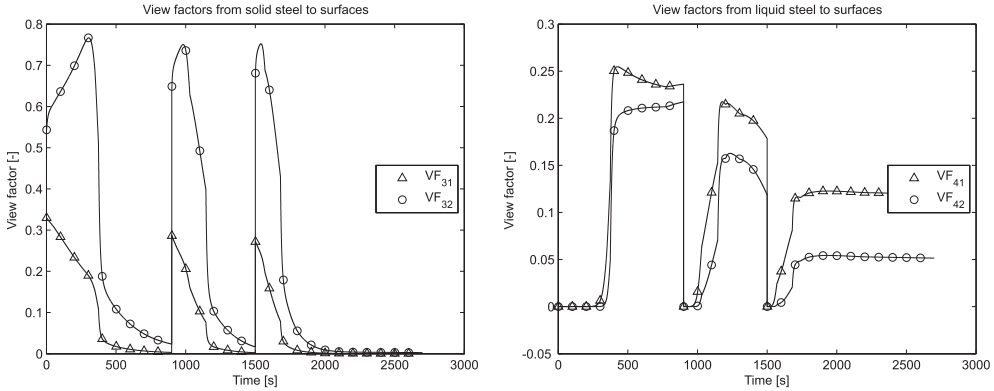

Fig. 4. Left panel: View factors from the solid steel to other surfaces in the EAF; Right panel: View factors from the liquid steel to other surfaces in the EAF.

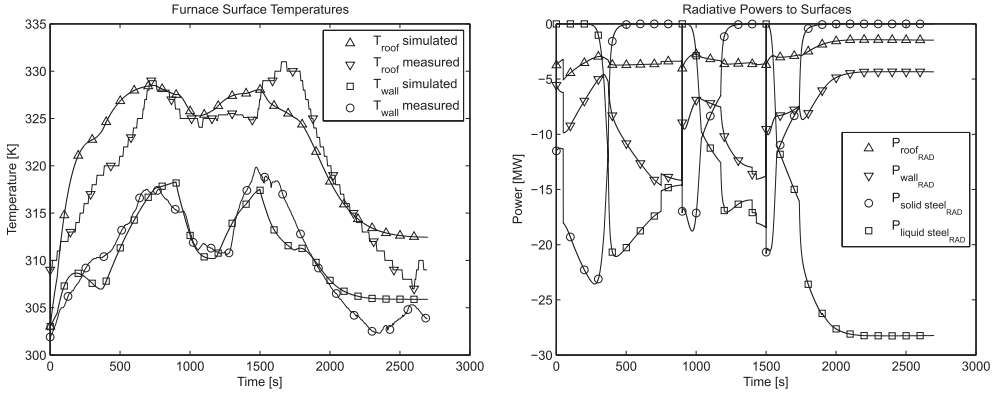

Fig. 5. Left panel: Comparison between measured and simulated temperatures of the furnace roof and water-cooled panels; Right panel: total radiative powers of each surface.

observed, which is also visible at VF_{3-2}. Both VFs drop to zero as the solid steel melts, while, on the other hand, VFs 4-1 and 4-2 appear from zero and increase with the amount of liquid steel. Like in the previous figures, lower values of VF_{4-1} and VF_{4-2} can be observed as the process approaches its end due to the foaming slag covering the steel bath.

To validate the presented modeling approach, simulated temperatures of the roof and wall cooling waters were compared to the operating measurements of the EAF, using the actual melting program for the simulation. Water temperatures were measured on each panel outlet (thermocouples); three outlets for the wall and one outlet for the roof area. Since the presented model considers the furnace vessel as a symmetrical shape, all three measured wall temperatures were averaged in order to compare them with simulated wall temperature.

The comparison between all the temperatures, together with the simulated sum of the radiative powers for each surface in the furnace, is shown in **Fig. 5**.

As is clear from Fig. 5, the water temperatures obtained with the proposed radiation model coincide with the obtained operational measurements, which suggests that the presented approach to the modeling of the radiative heat-transfer processes is sound and accurate. Temperature changes are mostly dependent on radiative heats to the surface, since the heat transferred from the gas zone amounts to only one-tenth of the total energy input to the roof and panels (low heat capacity of the gases) and the gas temperature is relatively stable (except at the beginning of each charge) around 1 850 K shown in fig. 7 of our previous study.[2] Also observable on the right panel are the radiative powers, which contain the inputs and outputs of the radiative energies to each surface. The negative characteristic of the curves denotes that the associated surface is receiving the radiative heat. Like in the previous figures an increased power to the liquid steel and a decreased power to the roof and panels can be observed when approaching the end of the heat as a consequence of the foaming slag.

4. Conclusion

In this paper an approach to the mathematical modeling of the radiative heat processes in electric-arc-furnace steelmaking is presented. The obtained model is developed in accordance with the fundamental laws of radiative heat transfer, a simplified EAF geometry and covers the major processes of radiative heat in the EAF. A simple EAF geometry is used due to the relatively complex acquisition of the view factors, which in the case of irregular surface shapes require extensive computational methods and therefore extend the complexity of the presented model. Moreover, in the case of such a complex system as an EAF, complex shape view factors would not necessarily yield better results nor could they be validated. The sources of the radiative heat in the EAF are assumed to be the surfaces with high temperatures and high emissivity factors, such as the arcs and the liquid bath, while other surfaces, like the roof, walls and solid steel, mostly receive radiative heat. Since the heat

exchange between some surfaces is either low due to the low temperatures of the surfaces (roof to walls) or it prevails in a conductive form (liquid to solid steel), these relations are omitted in the presented model. The parametrization of the model is carried out using both the available theoretical data for the EAF heat processes and the online measurements of the temperatures of the water-cooled panels. The presented model complements the complete EAF model,[1–3] which describes most of the physical processes during the EAF recycling, but was not included to these publications at that point because of the length and for an easier understanding of the papers. The goal of the presented EAF modeling is to obtain a relatively reliable radiation model, which plays and important role in the overall EAF model, especially when using these models in optimization procedures.

Acknowledgement

The work presented in this paper was funded by Slovenian Research Agency (ARRS) project *J* 2 – 2310 *Monitoring and Control of Steel Melt Quality in Electric Arc Furnace*.

REFERENCES

1) V. Logar, D. Dovžan and I. Škrjanc: *ISIJ Int.*, **51** (2011), No. 3, 382.
2) V. Logar, D. Dovžan and I. Škrjanc: *ISIJ Int.*, **52** (2012), No. 3, 402.
3) V. Logar, D. Dovžan and I. Škrjanc: *ISIJ Int.*, **52** (2012), No. 3, 413.
4) R. D. M. MacRosty and C. L. E. Swartz: *Ind. Eng. Chem. Res.*, **44** (2005), No. 21, 8067.
5) J. A. T. Jones, B. Bowman and P. A. Lefrank: The Making, Shaping and Treating of Steel, 10th ed., Chapter 10: Electric Furnace Steelmaking, The AISE Steel Foundation, Pittsburgh, PA, USA, (1998), 525.
6) R. Siegel and J. R. Howell: Thermal Radiation Heat Transfer, Taylor and Francis, Washington, USA, (2001).
7) A. Feingold: *J. Heat Transf.*, **100** (1978), No. 4, 742.
8) M. H. N. Naraghi and B. T. F. Chung: *J. Heat Transf.*, **104** (1982), No. 3, 426.
9) A. J. Buschman and C. M. Pittman: Configuration Factors for Exchange of Radiant Energy between Axisymmetrical Sections of Cylinders, Cones, and Hemispheres and their Bases, National Aeronautics and Space Administration, Washington, USA, (1961).
10) H. Brockmann: *Int. J. Heat Mass Transf.*, **37** (1994), No. 7, 1095.
11) S. N. Rea: *AIAA J.*, **13** (1975), No. 8, 1122.
12) K. N. Shukla and D. Ghosh: *Indian J. Heat Transf.*, **23** (1985), 244.
13) H. Matsuura and R. J. Fruehan: *ISIJ Int.*, **49** (2009), No. 10, 1530.